ELECTROSTATIC PLASMA INSTABILITIES IN HIGHLY ACTIVE AURORA OBSERVED BY A SOUNDING ROCKET S-310JA-7

Tadahiko OGAWA,

Hiraiso Branch, Radio Research Laboratories, 3601 Isozaki, Nakaminato-shi, Ibaraki 311-12

Hirotaka MORI, Shigeru MIYAZAKI

Radio Research Laboratories, Nukui-Kitamachi 4-chome, Koganei-shi, Tokyo 184

and

Hisao YAMAGISHI

National Institute of Polar Research, 9-10, Kaga 1-chome, Itabashi-ku, Tokyo 173

Abstract: A sounding rocket S-310JA-7 launched from Syowa Station, Antarctica, carried into highly active auroras the Faraday cup for measuring electron density fluctuations of both 5–330 Hz and 0.1–8 kHz bands together with electron density and precipitating electron flux above 105 eV. There existed two important irregular regions caused by electrostatic plasma instabilities. At altitudes of 100–140 km both cross-field (gradient-drift) and two-stream instabilities were found, the excitation of which depends on the strength of DC electric field; the two-stream instability giving rise to high-frequency fluctuations becomes important when $E \gtrsim 25$ mV/m, while the cross-field instability exciting longer wavelengths is dominant when $E \lesssim 25$ mV/m. Electrostatic ion cyclotron waves (frequency $\simeq$38–45 Hz, frequency bandwidth $\simeq$10 Hz) propagating nearly parallel to the auroral form were observed around a 200 km altitude in association with strong field-aligned currents. Additionally, artificially modulated fluctuations due to the plasma wake produced by rocket body and other probes were detected.

These results are discussed in the light of recent theories of electrostatic plasma instabilities in the auroral ionosphere.

1. Introduction

It is well known that the auroral ionosphere is not always quiescent but sometimes is disturbed to form small-scale, irregular fluctuations ($<$100 m) of both electron density and electric field, especially during the disturbed period (*e.g.*, FEJER and KELLEY, 1980). A few rocket experiments indicate that electrostatic fluctuations in the auroral ionosphere are due to some plasma instability processes, that is, two-stream and cross-field (gradient-drift) instabilities, operating under the conditions of strong electric field and/or inhomogeneous electron density distributions associated

with auroral activity (KELLEY and MOZER, 1973; OGAWA *et al.*, 1975, 1976). The electrostatic ion cyclotron instability excited by strong field-aligned currents is believed to become important in higher regions above *F*-layer from theory (KINDEL and KENNEL, 1971) and from observation (BERING *et al.*, 1975). Recently, this instability has been invoked for a theoretical explanation of a certain type of *E*-region irregularities (D'ANGELO, 1973; CHATURVEDI, 1976).

The *in-situ* measurements of these fluctuations in aurora have been few up to now. The reasons may be that rocket payloads must be highly sophisticated and assembled appropriately in order to clarify the causal mechanisms and moreover that rocket must penetrate into active auroras in order to get useful and stimulating information. The observation satisfying these requirements has been made in 1978 at Syowa Station, Antarctica, by a rocket S-310JA-7. As one of the missions for the fluctuation measurement, a Faraday cup which measures DC and AC elctron density (two frequency-bands, 5–330 Hz and 0.1–8 kHz) and precipitating electron flux above 105 eV was flown into highly active auroras. Also both DC and AC electric fields (<220 Hz) were measured along with the density measurement (OGAWA *et al.*, 1981; YAMAGISHI *et al.*, 1981).

The purpose of this paper is to present what kinds of instabilities take place during auroral display in association with strong electric fields and with intense electron precipitation along the geomagnetic field line. In addition to the natural fluctuations due to the plasma instabilities, artificially modulated fluctuations due to the wake generated by other probes were also found at certain altitudes.

2. Instrumentation

Block diagram for the measurement is presented in Fig. 1. The Faraday cup, 100 mm in diameter and 36 mm in height, consists of four meshed-grids (G1 to G4) using thin tungsten wires and one collector, each of which is plated with gold. Appropriate DC voltages as shown in Fig. 1 are applied to the grids and collector for detecting only electron-current component. The output from Grid 1 is sent to the IRIG telemetry channel No. 10 through the logarithmic amplifier and is analyzed to get background electron density distribution. Grid 1 is used also by other experimenter for detecting HF-band fluctuation (PWN-H).

The output from Grid 2 is divided into two fluctuating components; one is low-frequency component of 5–330 Hz (PWN-L) and the other is high-frequency one of 0.1–8 kHz (PWN-W). The PWN-W circuit has a function of automatic gain control (AGC). A nearly monochromatic frequency between 2 and 8 kHz corresponding to AGC level is superposed upon the output from Grid 2.

A DC voltage of -105 V is applied to Grid 4, by which precipitating electrons having energies beyond 105 eV can be collected mostly by the collector. The current proportional to energetic electron flux is amplified logarithmically and then sent to

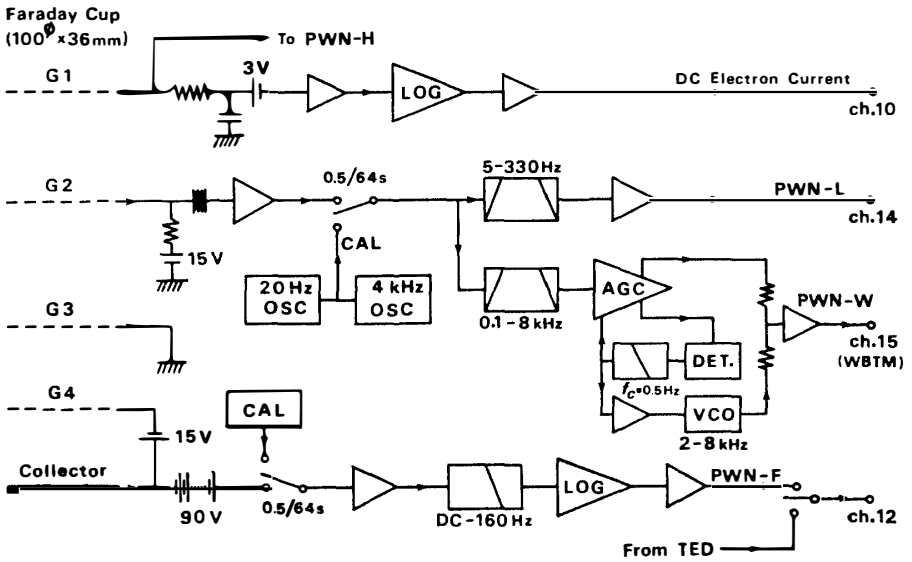

Fig. 1. Block diagram of the PWN-L, -W and -F payloads aboard S-310JA-7.

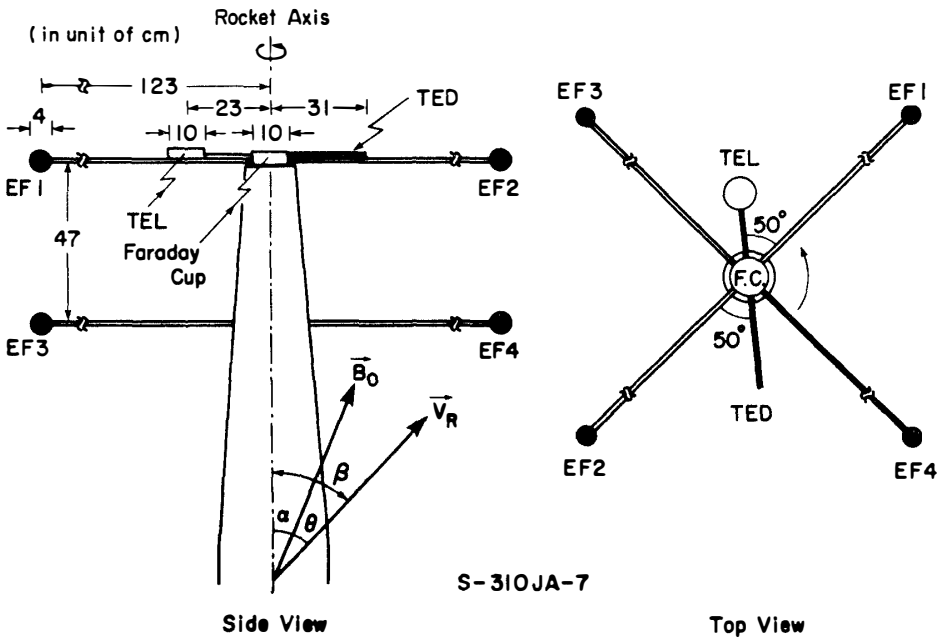

Fig. 2. Top (right) and side (left) views of the probe arrangement for S-310JA-7 measurement of electric field (EF1–EF4), electron temperature (TEL) and energy distribution of thermal electrons (TED). Faraday cup (F.C.) is placed on the top of rocket body.

the telemetry channel No. 12 (PWN-F) which is time-shared every two seconds with measurement of energy distribution function of thermal electrons (TED) by other experimenter. Secondary electrons below 15 eV emitted from the collector is repulsed again to the collector by a relative voltage of -15 V which is applied to Grid 4. Grid 3 is inserted to prevent mutual interference between the upper two grids and G4 and collector.

Normal operation of the PWN-L, -W and -F circuits is checked for 0.5 s every 64 s. The Faraday cup was installed at the top of rocket body as shown in Fig. 2 in order to avoid any disturbance due to rocket motion as far as possible.

3. Observation

The S-310JA-7 rocket was launched geomagnetically northward (equatorward) at 2215:50 LT (45°EMT) on March 27, 1978 from Syowa Station, aiming at a southward-moving auroral arc in the northern sky. For later reference, time variation of the rocket attitude during the flight is presented in Fig. 3 in which the angle α between the rocket axis and the geomagnetic field vector $\boldsymbol{B}_0$ was obtained from the on-board geomagnetic aspect-sensor while the angle θ between $\boldsymbol{B}_0$ and rocket velocity vector $\boldsymbol{V}_R$ was calculated by using the recent $\boldsymbol{B}_0$ model and the rocket trajectory data. The angle θ is drawn by the continuous curve. Since absolute attitude of the rocket was not determined, a possible range of β (angle between rocket axis and $\boldsymbol{V}_R$) is represented

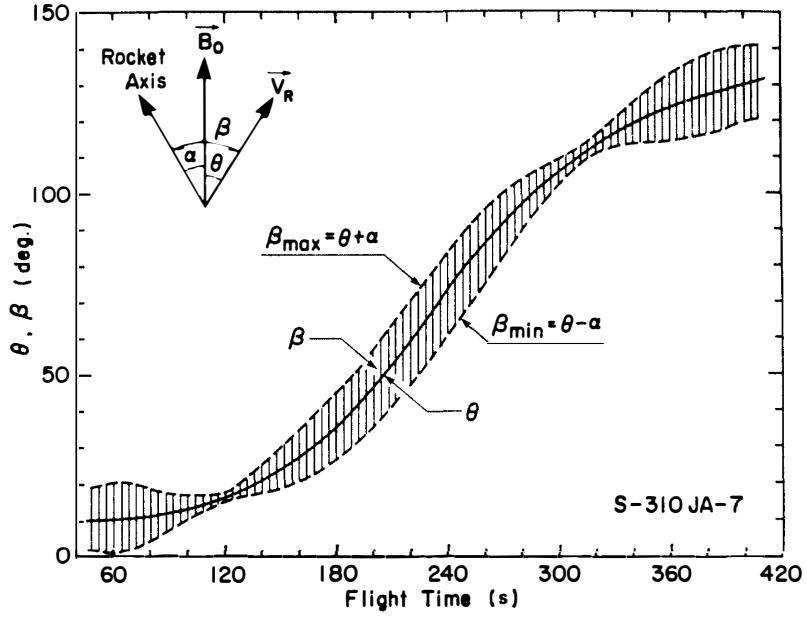

Fig. 3. Time variations of θ and β which are defined in the figure. Since α is not determined uniquely, possible range of β is shown by the vertical bar.

by the vertical bar. Maximum and minimum of β, β_{max} and β_{min}, respectively, are represented by the dashed-curve.

3.1. Aurora

Fig. 4 illustrates contour maps of auroral 5577 Å (upper panel) and H_β (lower panel) intensities which were constructed from the meridian scanning-photometer measurement at Syowa Station. Note that one scan needs 30 s and that a lower border of auroral heights is assumed to be about 100 km. Also shown is the rocket trajectory projected onto the 100 km altitude along the geomagnetic field line.

Just after the launching, a substorm expansion phase ($\Delta H \simeq -740\gamma$, 30 MHz CNA$\simeq$3.9 dB) and a rapid southward-movement of the bright arc started almost simultaneously. Fig. 4 together with the all-sky photographs taken every 10 s at Syowa Station indicates the following. The ascending rocket began to encounter with the 25–35 kR arc at the flight time of about 70 s (2217:00 LT) and flew within it

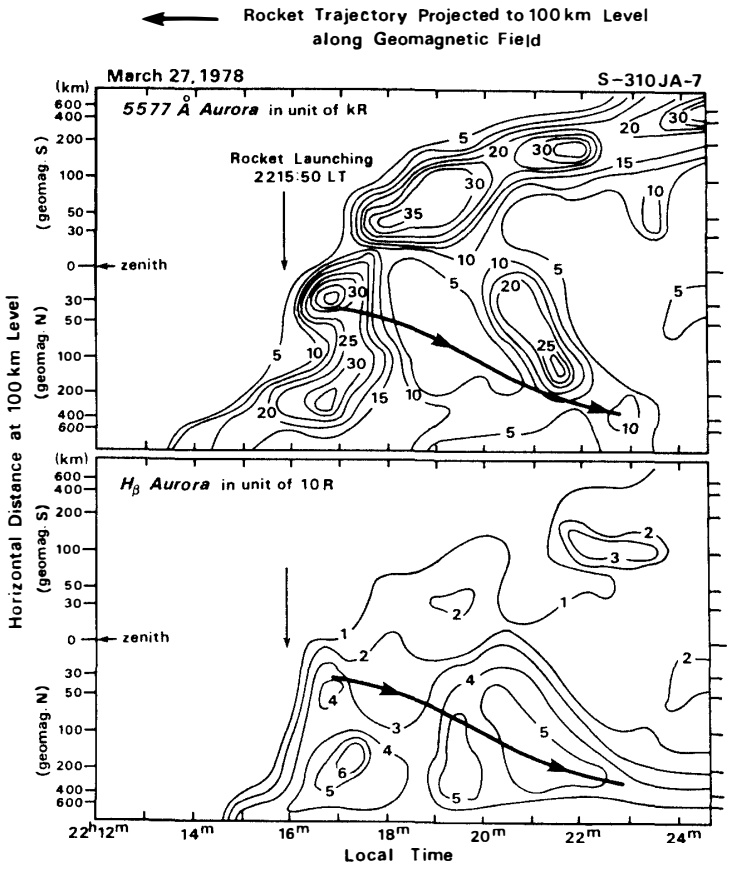

Fig. 4. Time profiles of 5577 Å (upper panel) and H_β (lower panel) intensities measured by meridian scanning-photometer at Syowa Station (courtesy of T. HIRASAWA). It takes 30 s for one scan. Also shown is the rocket trajectory projected onto the 100 km altitude along the geomagnetic field.

until 100 s (2217:30 LT). This southward-moving arc passed over Syowa Station and then split into two arcs at 210 s (2219:20 LT) as recognized in Fig. 4. After the split, one arc moved further toward south while the other moved back over Syowa Station and then toward the rocket. The latter arc started at about 270 s (2220:20 LT) to be changed into a large-scale, eastward-traveling spiral structure. The descending rocket flew near the northward edge of this structure during 270–320 s (2221:10 LT). After 320 s the rocket was far from the spiral structure which had moved away eastward, but still was near the northward side of the northward-moving arc which is a tail extending from the spiral structure (see Fig. 4). The aurora after 370 s (2222:00 LT) was faint near the rocket.

3.2. Electron density and energetic electron precipitation

The lower panel in Fig. 5 shows the time profiles of electron density (N_e) and probe current by energetic electrons above 105 eV (J_p). It is interesting to compare these profiles with Fig. 4. As described above, the rocket was within the 25–35 kR aurora during 70–100 s (100.4–140.6 km). Correspondingly, the maximum of the electron density N_e was about $9.4 \times 10^5/\text{cm}^3$ at 88 s (125.5 km), the value of which is highest among the past rocket experiments at Syowa Station (OGAWA *et al.*, 1978). Additionally the second peak at about 62 s (88.3 km) is attributed to the D-region ionization due to highly-energetic precipitating electrons (<several hundred keV). N_e decreased with time (that is, with altitude) outside the active aurora and reached

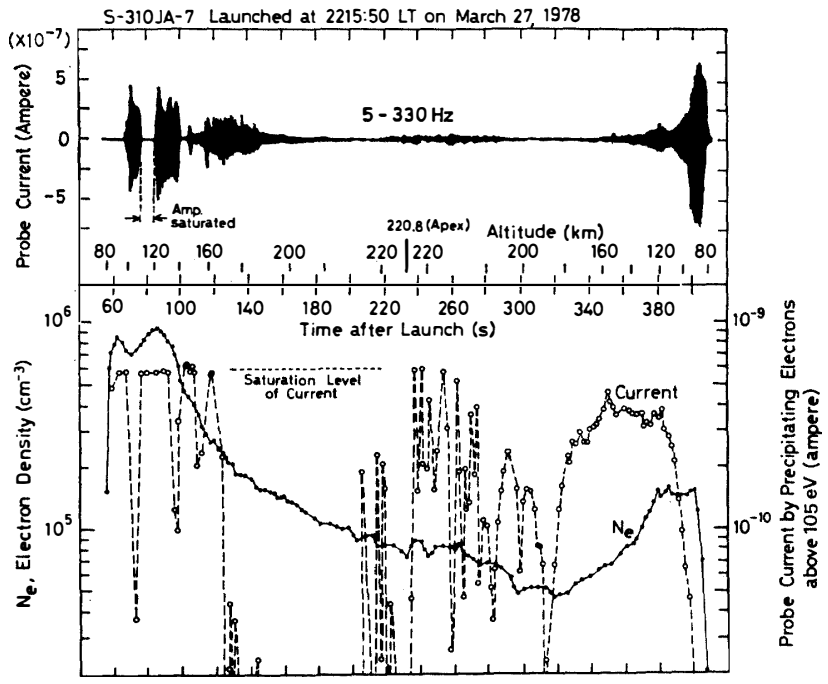

Fig. 5. Time variations of 5–330 Hz fluctuation component (upper panel), electron density and probe current by precipitating electrons above 105 eV (lower panel).

the minimum value of $5 \times 10^4/cm^3$ at about 320 s (186.8 km) in the descent, followed by the gradual increase as approaching the northward-moving arc (see Fig. 4). The E-region N_e during the descent was about $1.6 \times 10^5/cm^3$. See a paper by MIYAZAKI *et al.* (1981) for detailed discussion on the electron density profile.

The electronics for detecting J_p was sometimes saturated during 63–110 s because of vast precipitation that caused the bright arc. Time-varying, irregular profile of J_p (and also of N_e) between 210 and 310 s indicates that the precipitation pattern was highly variable in time and space, at least near the northward edge of the eastward-traveling spiral structure of aurora (see Subsection 3.1). Auroral structure associated with this behavior cannot be explicitly seen in Fig. 4. J_p increased again after 310 s as the rocket approaching the northward-moving arc but is not so high as that measured during the ascent. We note that α defined in Fig. 3 was between 1° and 12° during 60–400 s so that J_p was mainly due to precipitating electrons coming down almost along the field line. Electron flux $F(>105$ eV) can be derived from an equation of $F=\varepsilon J_p/Se$ where S is the area of the collector, e the electronic charge and ε the inverse of transparence efficiency of the four grids, G1 to G4. Though ε was not measured exactly before launch, it is estimated to be about 2.5 which is derived only from consideration of the structure of the grids. These make $F \simeq 3.4 \times 10^{17} J_p$ electrons/cm^2·s (J_p in ampere). We do not know, however, what happened during the flight to modify ε by the bombardment of high energy electrons. Therefore F derived from the above equation should be regarded as a rough estimation. We confirm, however, that the time profile of J_p as presented in Fig. 5 reflects well the behavior of the precipitating electron flux.

3.3. Electron density fluctuation of 5–330 Hz band

Chart recording of 5–330 Hz electron density fluctuation is reproduced in the upper panel in Fig. 5. It should be noted that during 77–86 s the pre-amplifier of Grid 2 was saturated due to very intense fluctuation so that the output from the 5–330 Hz band-pass filter dropped nearly to zero level. The AC electric field detector measured strong fluctuation during this time interval (YAMAGISHI *et al.*, 1981). It is seen in Fig. 5 that there exist four time intervals in which the low-frequency fluctuations appear; 68–100 s, 110–160 s, 230–290 s and 350–410 s. Close examination of the telemetry data shows that the fluctuations during 350–410 s are exclusively due to the rocket wake because β was between 115° and 140° (see Fig. 3). Similarly, the fluctuations during 110–160 s are not natural but are identified to be due to the disturbances produced by the probes of TEL and TED. These fluctuations will be discussed in somewhat detail in the later section.

4. Data Analysis

In this section the characteristics of 5–330 Hz and 0.1–8 kHz density fluctuations

are presented and their possible generation mechanisms are discussed by using the DC electric field and precipitating electric flux data. Frequency *power* spectrum, the spectral peak of which is normalized to unity, was calculated by applying a technique of 128-point FFT (fast Fourier transform, frequency resolution$\simeq$7.81 Hz), unless otherwise noted, after analog-to-digital conversion of tape-recorded analog telemetry-output. The integration time for getting one spectrum is about 2 s.

Fig. 6 illustrates some representative spectra of 5–330 Hz fluctuations during the whole flight. The spectrum with intense fluctuation amplitude (see upper panel in Fig. 5) is shaded with gray in the figure. Specially noted is that the spectra during 92–100 s (130–140 km) have a tendency of flatness while the other shaded-spectra decrease in amplitude with frequency. Another interesting feature in Fig. 6 is the sharp peak appeared in the spectrum at about 280 s (211 km). Later this peak will be identified to be due to the electrostatic ion cyclotron instability.

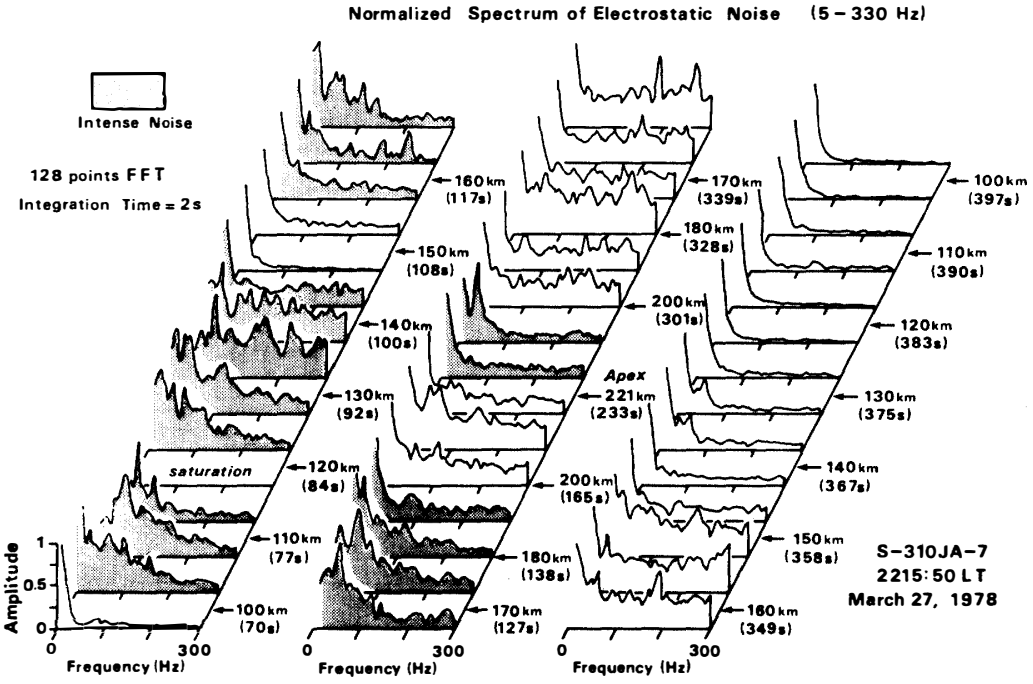

Fig. 6. Some representative spectra of 5–330 Hz fluctuations during the whole flight. Each spectrum is normalized so that maximum amplitude is unity. The spectrum with intense fluctuation amplitude is shaded with gray.

4.1. Fluctuations during 68–100 s (97–141 km)

Fluctuations during 68–100 s are very interesting because the rocket was within the highly active aurora which is characterized by both the 25–35 k*R* 5577 Å brightness and the high electron density associated with strong precipitation. Fig. 7 shows spectrogram of 0.1–8 kHz fluctuation (top panel), computer-plot of 5–330 Hz fluctuation component (second panel), DC electric field strength and its direction in geo-

magnetic coordinates (third panel) and electron density (bottom panel). We note in the top panel, where the 0.1–8 kHz signal is represented by the white portion, that the dot-like structure between 4 and 7 kHz modulated with the rocket spin period ($\simeq$1.1 s) is artificial because this structure is seen in the spectrogram during the whole flight, and that the relatively weak signal (not explicitly recognized in the figure) appearing below 4 kHz continued also during the whole flight. Causal mechanism of the former structure is not known well. The latter continuous spectrum can be understood partly as a result of the AGC function of the PWN-W circuit (see Section 2) by which the weak signal-input to the circuit is sufficiently amplified. If this function did not exist, the continuous spectrum below 4 kHz could not appear or would be much weaker.

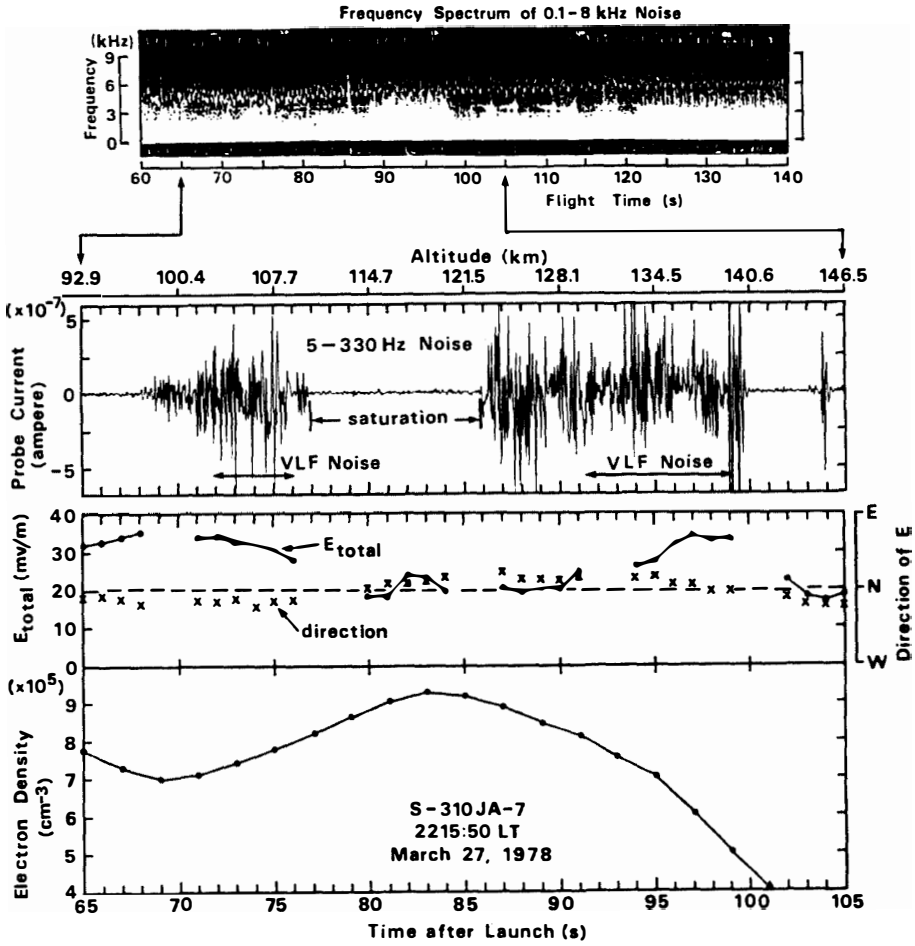

Fig. 7. Close-up of 0.1–8 kHz fluctuation spectrogram (top panel) 5–330 Hz fluctuation component (second panel), DC electric field and its direction (third panel, courtesy of T. OGAWA), and electron density (bottom panel) during 65–105 s. The time interval during which strong fluctuations beyond 3 kHz appeared is represented as "VLF Noise" in the second panel.

The time interval during which the fluctuations having strong spectral components exceeding 3 kHz appeared is represented as "VLF Noise" in the second panel in Fig. 7. The spectral forms during "VLF Noise" are largely different from those at any other times. The spectra between 90 and 98 s are more interesting than those at about 74 s from the viewpoint of signal strength and frequency extent and therefore will be discussed later together with the 5–330 Hz spectra (see Fig. 9).

Some spectra of the 5–330 Hz fluctuations covering the period presented in Fig. 7 are shown in Fig. 8. When the fluctuation amplitudes are relatively low during 68.6–72.5 s before the first "VLF Noise" detection, the spectral power drops sharply with frequency, say f^{-2}, f being the frequency. Subsequently, when the amplitudes become high after 72.5 s, the spectra are roughly flat below 100 Hz and roll off with a form of approximately $f^{-1.6}$ toward higher frequency. The spectra become harder ($f^{-0.3}$) when the second strong "VLF Noise" appears as can be seen in the 89.8–91.8 s and 95.7–97.7 s spectra. The fluctuation energies are almost uniformly distributed within the frequency range of band-pass filter (BPF), suggesting thereby that the spectrum extends to a higher frequency range.

Fig. 9 illustrates time variations of the spectra of both 5–330 Hz (left panel) and 0.1–8 kHz fluctuations (right panel) during 90–100 s. It should be remarked in the right panel (a) that the shaded-peak at about 3 kHz is due to the AGC level super-

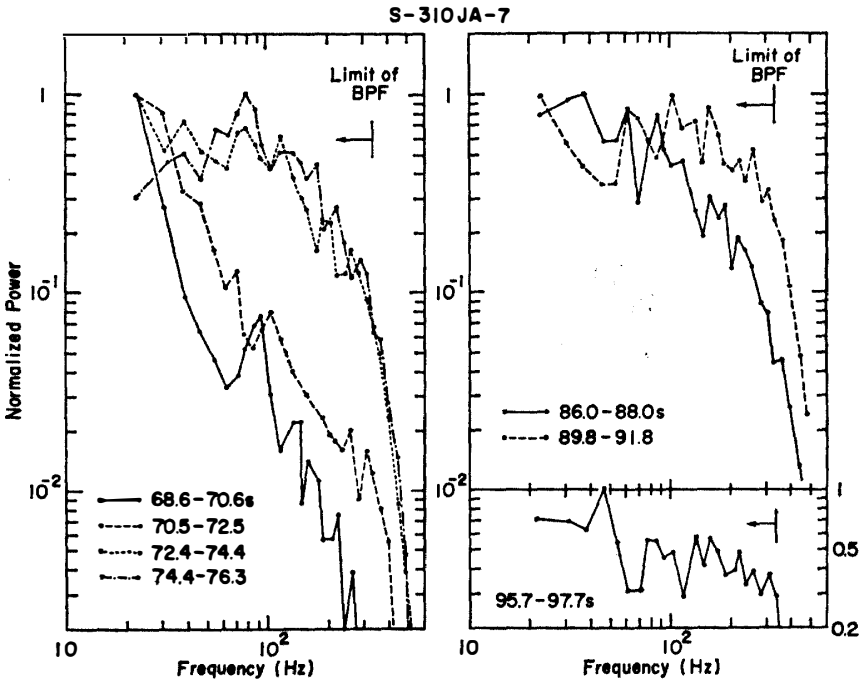

Fig. 8. Some frequency spectra of 5–330 Hz fluctuations during the times shown in Fig. 7. Spectral component beyond 330 Hz is outside a frequency-response of the band-pass filter (BPF).

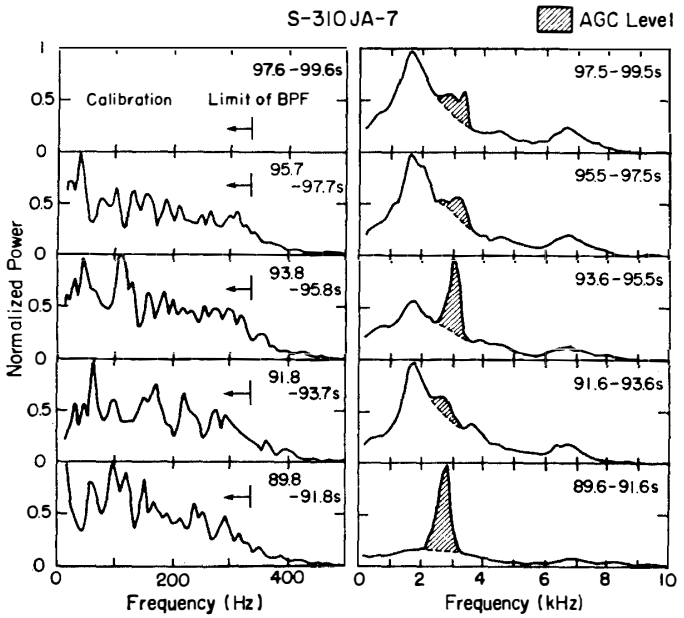

Fig. 9. Serial frequency spectra of 5–330 Hz (left panel) and 0.1–8 kHz (right panel) fluctuations when strong second "VLF Noise" appeared. See text as to the spectra in the right panel.

posed on the PWN-W signal (see Section 2), (b) that the broad peak between 6 and 7 kHz corresponds to the dot-like structure seen in Fig. 7, and (c) that the peak at about 1.6 kHz may be apparent because the sensitivity of the PWN-W circuit drops toward the low-frequency side below this frequency as well as toward the high-frequency side beyond 7 kHz. By considering these points and the spectral characteristics of 5–330 Hz spectra as seen previously, it is concluded that the fluctuations during 90–100 s have a continuous and smooth spectrum extending from a few Hz to about 5 kHz. The fluctuation amplitudes during 72–76 s are weaker and their frequency extents are below about 4 kHz.

The DC electric fields, E_{total}, are between 20 and 35 mV/m during 68–100 s and are almost geomagnetically northward as seen in the third panel in Fig. 7. We see that E_{total} is beyond 25 mV/m when the intense "VLF Noise" was observed. Electron drift velocity given by $\boldsymbol{V}_d \simeq \boldsymbol{E}_{total} \times \boldsymbol{B}_0/B_0^2$ becomes 580 m/s for $E_{total}=25$ mV/m, which exceeds the sound velocity $V_s(\simeq\sqrt{\kappa T_e/m_i})$ of about 500 m/s for $T_e=800$ K and NO^+ ion. This condition sets up the two-stream instability (*e.g.*, FARLEY, 1963) by which electron density fluctuations extending up to 10 kHz are excited (KELLEY and MOZER, 1973). These suggest that the intense fluctuations observed during the "VLF Noise" periods are due to the two-stream instability because E_{total} is beyond 25 mV/m during these periods.

When V_d is smaller than V_s, the cross-field instability is possible under the com-

bined action of electron density gradient and DC electric field which is much smaller than the critical field E_{cr} for the two-stream instability (SATO, 1971). The present experiment suggests $E_{cr} \simeq 25$ mV/m for an intense excitation of the two-stream instability.

We do not have any fluctuation data during 76–86 s because of the amplifier saturation. E_{total} is below E_{cr} during 76–91 s while N_e is largest, suggesting that the electric field is reduced in auroral arc (DE LA BEAUJARDIERE *et al.*, 1977; OGAWA *et al.*, 1981). It is supposed, therefore, that the AC electric field fluctuations observed during 77–86 s were due to the cross-field instability rather than the two-stream instability (YAMAGISHI *et al.*, 1981). In fact, the bottom panel in Fig. 7 indicates the existence of the electron density gradient parallel to E_{total} during 69–83 s. This fact favors an excitation of the cross-field instability (*e.g.*, SATO, 1971).

4.2. Fluctuations during 110–160 s (152–197 km)

We have noted in Subsection 3.3 that the fluctuations during 110–160 s are artificial. An example of computer-plot of the 5–330 Hz fluctuation component during 125.6–131.6 s is shown in Fig. 10, in which burst-like enhancements of the G2 probe current appear almost periodically with half the rocket spinning period of about 1.1 s though the duration of these increases with time. Amplitudes of these enhancements were largest around the time interval of 116–132 s (159–175 km) and decreased before and after these times. For explaining these, it is unnatural to assume that the irregular-layer existed periodically with altitude. Let us consider the probe arrangement shown in Fig. 2 where we see that the electron temperature (TEL) and TED probes are extended radially with the mutual angle of 180°. If the plasma flow direction

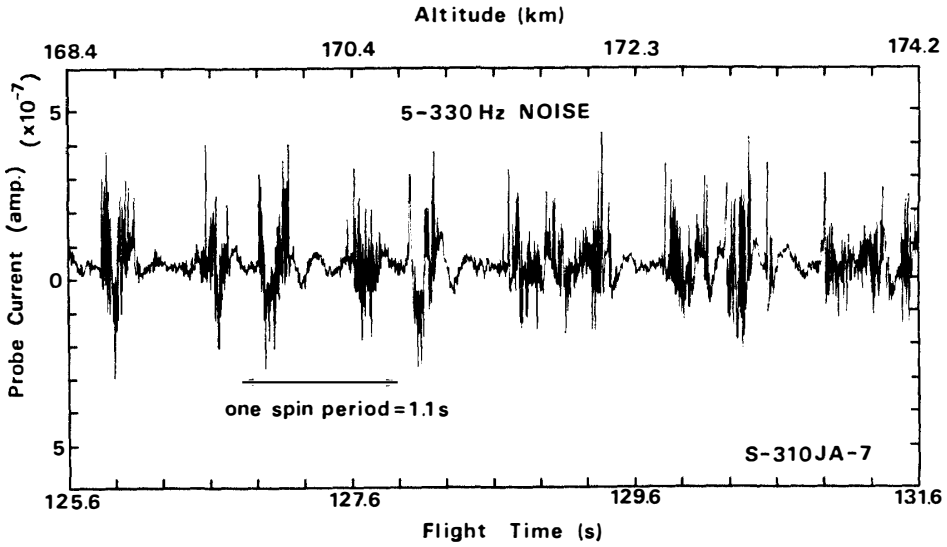

Fig. 10. Computer-plot of probe current of 5–330 Hz fluctuation component during 125.6–131.6 s.

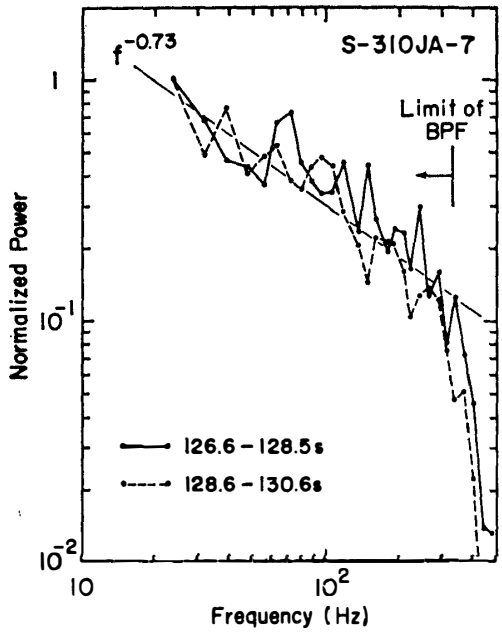

Fig. 11. Two frequency spectra during the time interval shown in Fig. 10.

due to both rocket motion and $\boldsymbol{E}_{total} \times \boldsymbol{B}_0$ drift in the rocket-fixed frame was nearly perpendicular to the rocket axis, disturbances produced by both probes would be periodically detected by the Faraday cup with half the rocket spinning period. Strictly speaking, the period of appearance of the enhanced fluctuation changed continuously with time during 110–160 s. Together with this, the increase in the duration time described above can be explained by the rocket attitude variation (see Fig. 3 for detail) and by the fact that E_{total} was changing its direction from north to west while increasing its strength (OGAWA *et al.*, 1981).

Fig. 11 presents two frequency spectra for the fluctuations shown in Fig. 10. As can be seen, these are approximated by a form of $f^{-0.73}$ within the frequency range of BPF. We do not know at this stage what detailed mechanism operated for generating such a spectral form.

4.3. Fluctuations during 230–290 s (221–206 km)

There existed the third irregular region just after passing the apogee (233 s, 220.8 km) until 290 s (206 km). The fluctuations are characterized by somewhat irregular and low-frequency oscillation ($f<20$ Hz) with low amplitude during 230–270 s and thereafter by quasi-sinusoidal oscillation. The spectra computed every 2 s during 269–290 s by using a 512-point FFT (frequency resolution $\simeq 1.95$ Hz) are presented in Fig. 12. This figure shows that the spectral peaks appear around $f_{obs}=$ 40 Hz with a very narrow bandwidth ($\sim$10 Hz). Note that the O^+ gyrofrequency, $f_H(O^+)$, is about 38 Hz for $B_0=0.4$ Gauss at altitudes around 200 km.

The irregular and sufficient electron precipitations (field-aligned currents) as

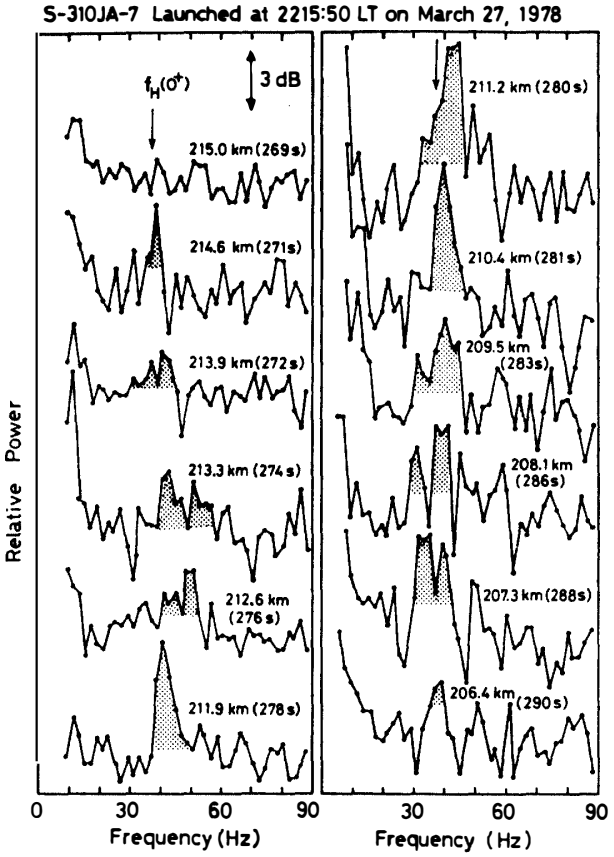

Fig. 12. Serial frequency spectra of 5–330 Hz fluctuations during 269–290 s. Note that the vertical scale is logarithmic. The O^+ gyrofrequency $f_H(O^+)=38$ Hz is shown in the figure by the arrow.

shown in Fig. 5, in addition to the above two facts (narrow band-width and spectral peak near but above $f_H(O^+)$), lead us to the hypothesis that the waves were produced by the electrostatic ion cyclotron instability which has been studied theoretically by KINDEL and KENNEL (1971). They showed that field-aligned flux of 10^9–10^{10} electron/cm^2·s or more at the 200 km altitude will destabilize the topside ionosphere to excite the waves propagating almost normally to $\boldsymbol{B}_0$ and having critical frequency $f \simeq f_H(O^+)$ for $T_e/T_i \ll 1$, $f \simeq 1.2 f_H(O^+)$ for $T_e/T_i \simeq 1$ and $f \simeq 1.5 f_H(O^+)$ for $T_e/T_i \gg 1$. The growth rate peaks at the perpendicular wavenumber given by $K_\perp^2 \rho_i^2 \simeq 1 \sim 2$ where ρ_i is the gyroradius which is about 3 m for $T_i \simeq 1000$ K. Phase velocities of the waves, $V_{ph}(=\omega/K_\perp)$, are between 584 and 700 m/s for $\omega \simeq (1.0\text{–}1.2)\omega_H(O^+)$ if $K_\perp^2 \rho_i^2 = 1.5$ is taken as a typical value.

The rocket velocity vector $\boldsymbol{V}_R$ during 270–290 s was nearly perpendicular to $\boldsymbol{B}_0$ ($\theta = 91°$–$102°$) with $V_R \simeq 840$ m/s (see Fig. 3). Since the ion cyclotron waves propagate in the plane almost normal to $\boldsymbol{B}_0$ ($K_\perp^2 \gg K_\parallel^2$) and since their phase velocities are comparable to V_R, we must take into account V_R as well as the plasma

flow vector $\boldsymbol{V}_F$ caused by $\boldsymbol{E}_{total} \times \boldsymbol{B}_O$ drift in order to relate ω_{obs} in the rocket frame with ω in the plasma frame. Then the following relation must be satisfied.

$$\omega_{obs} = \omega + \boldsymbol{K}_\perp \cdot (\boldsymbol{V}_R + \boldsymbol{V}_F). \tag{1}$$

$\boldsymbol{V}_F$ was estimated to be geomagnetically northward with $V_F = 1500$ m/s corresponding to the westward electric field of $E_{total} = 60$ mV/m (OGAWA *et al.*, 1981) while $\boldsymbol{V}_R$ relative to the rocket frame was southward. By using $K_\perp = 0.408$/m, these reduce eq. (1) to

$$f_{obs} = f + 42\cos\delta, \tag{2}$$

where δ is the angle between $\boldsymbol{K}_\perp$ and the geomagnetic north direction. The observation presented in Fig. 12 shows $f_{obs} = 38 \sim 45$ Hz $\simeq (1.0\text{–}1.2) f_H(O^+)$, which indicates from eq. (2) that δ should be within $90 \pm 6°$ ($\cos\delta = \pm 0.1$). This direction is almost parallel to the northward edge of the large-scale, eastward-traveling spiral structure of aurora (see Subsection 3.1) and also to the electric field.

Let us consider NO^+ ions instead of O^+ ions, for which eq. (2) is written as

$$f_{obs} = f + 58\cos\delta. \tag{3}$$

For this case, $f = (1.0\text{–}1.2) f_H(NO^+) = 20\text{–}24$ Hz, so that $\delta = 70°$ to satisfy eq. (3). This result does not change essentially the above description concerning $\boldsymbol{K}_\perp$.

5. Discussion

It has been found that the cross-field and two-stream instabilities took place at altitudes of 100–140 km in the active aurora where a strong electrojet current flows. These instabilities belong to the same dispersion relation (SUDAN *et al.*, 1973), which tells that the two-stream instability condition for growth is given by $V_d \gtrsim V_s$ when the density gradient is ignored and that at long wavelengths the cross-field instability becomes important even if $V_d \lesssim V_s$ since the gradient term contributes to drive this instability. Our observation confirms that when $E \gtrsim 25$ mV/m the two-stream instability is excited resulting in the spectrum which has frequency component up to 5 kHz (Fig. 9). When $E \lesssim 25$ mV/m, wavelengths excited by the cross-field instability become so long that the wave energy is concentrated in the lower frequency range (Fig. 8). The critical electric field of $E_{cr} = 25$ mV/m for the growth of the two-stream instability is consistent with the result by simultaneous observations of auroral echoes with the 398 MHz radar at Homer, Alaska and electric field with the Chatanika incoherent scatter radar (MOORCROFT, 1979).

Non-linear studies of the cross-field instability tell that the two-dimensional frequency spectrum $P(f)$ should obey a form of $P(f) \simeq f^{-3}$ (*e.g.*, SATO, 1971; MCDONALD *et al.*, 1974; SATO and OGAWA, 1976; SUDAN and KESKINEN, 1979). Our results indicate, however, $P(f) \simeq f^{-2}$ during 68.6–72.5 s and at other times $P(f) \simeq f^0$ below 100

Hz and $P(f) \simeq f^{-1.6}$ between 100–330 Hz. The above theories permit two-dimensional wave propagation in the plane normal to $\boldsymbol{B}_0$, assuming $K_{\parallel} = 0$. Since the ascending rocket flew nearly along $\boldsymbol{B}_0$ in the E-region (see Fig. 3), our spectral forms should not be compared directly with a theoretical form of f^{-3} and rather indicate that there existed waves propagating parallel to $\boldsymbol{B}_0$ ($K_{\parallel} \neq 0$) in very active aurora. This may cast a doubt on the usual assumption that electron density irregularities are field-aligned.

The irregularity-layer caused by the above plasma instabilities was between 97–141 km, which is wider than the thickness observed by KELLEY and MOZER (1973) and OGAWA *et al.* (1976). This result shows that the vertical extent of the auroral electrojet current becomes wider in a very active aurora because of the strong electric field than in a moderate or quiet aurora.

Electrostatic ion cyclotron waves generated by the precipitating particles have been found at altitudes of 206–215 km during the descent. The present result indicates that the propagation vectors are almost parallel to the auroral form, while BERING *et al.* (1975) observed in the F-layer (385 km) these waves propagating almost normally to auroral arc. Usual theories of collisionless ion cyclotron instability (*e.g.*, KINDEL and KENNEL, 1971) permit omni-directional propagation in the plane perpendicular to $\boldsymbol{B}_0$, which is inconsistent with the above observations. HENDEL and YAMADA (1974), however, pointed out that propagation perpendicular to local density gradient is possible. This situation may be appropriate to the present case since the density gradient perpendicular to the aurora is possible judging from the all-sky photographs. Final answer to this problem, however, must wait until more data are accumulated in the future.

Precipitating electron fluxes above 105 eV observed in association with the ion cyclotron waves were of the order of $F = 10^8$–10^9 electrons/cm^2·s (see Fig. 5 and Subsection 3.2). These fluxes are smaller than that given by KINDEL and KENNEL (1971) who predict $F = 10^9$–10^{10} electrons/cm^2·s for the growth in the topside ionosphere (CLOUTIER *et al.*, 1973). We point out two reasons for this discrepancy; one is due to the estimation of transparence efficiency ε (see Subsection 3.2 for detail) and the other is due to that the lower-limit of electron energies (105 eV) to be detected might be too high to get information of the precipitating flux in a full energy range. CHATURVEDI (1976) has discussed the role of collision frequencies on excitation of ion cyclotron instability in the F-region, whereas the theory by KINDEL and KENNEL (1971) is applied to the case of weak collision and therefore to regions above F-layer peak. This indicates that we may not be able to ignore the collisional effect at altitudes around 200 km in considering the threshold flux. Further discussion on this matter, however, is beyond the scope of this paper.

D'ANGELO (1973) and CHATURVEDI (1976) have proposed collisional ion cyclotron instability for explaining a certain type of VHF auroral radar echoes which return from electron density irregularities in the E-region. In the present case, this insta-

bility cannot be distinguished from other instabilities, even if it operated, because the spectral peak ($\sim$20 Hz for NO^+) of cyclotron waves is buried in the spectrum due to the two-stream and cross-field instabilities.

6. Conclusion

The following results are obtained by *in situ* electron density fluctuation measurement in highly active auroras.

(1) The fluctuations caused by the two-stream and cross-field instabilities were found at altitudes of 100–140 km. Critical electric field for separating these instabilities is about 25 mV/m. Frequency spectra of the 5–330 Hz fluctuations obey a form of $f^{-2}\sim f^{-1.6}$, varying with altitude. The spectra extend up to 5 kHz when $E\gtrsim$25 mV/m (two-stream instability condition). Our results indicate that the waves propagating parallel to the geomagnetic field existed, contrary to the usual assumption that electron density irregularities are field-aligned.

(2) The electrostatic ion cyclotron waves (O^+ or NO^+) excited by the field-aligned current were detected around 200 km altitude during the rocket descent. The spectra have a sharp peak around 38–45 Hz with the spectral width of about 10 Hz. These waves seem to have propagated both nearly parallel to the auroral form and perpendicular to $\boldsymbol{B}_0$ though theory predicts no preferred direction in the plane normal to $\boldsymbol{B}_0$.

(3) The 5–330 Hz fluctuations having a spectral form of $f^{-0.73}$ during 110–160 s are identified to be due to the wake produced by other probes. Detailed mechanism of these fluctuations is unknown. The wake effect due to rocket body was found during 350–410 s in the descending. Frequencies of these fluctuations are limited below 30 Hz, unlike the fluctuations during 110–160 s.

Acknowledgments

We would like to express our sincere thanks to the members of the wintering party of the 19th Japanese Antarctic Research Expedition, headed by Prof. T. HIRASAWA, for their painful effort for rocket launching and data collection under severe conditions. We are also grateful to Prof. T. OGAWA of Kyoto University for providing the DC electric field data. Many thanks are due to Messrs. M. OSE and K. IGARASHI of the Radio Research Laboratories for their support to the experiment.

This experiment was conducted as one of the special projects of the National Institute of Polar Research during the IMS period.

References

BERING, E. A., KELLEY, M. C. and MOZER, F. S. (1975): Observations of an intense field-aligned thermal ion flow and associated intense narrow band electric field oscillations. J. Geophys. Res., **80**, 4612–4620.

CHATURVEDI, P. K. (1976): Collisional ion cyclotron waves in the auroral ionosphere. J. Geophys. Res., **81**, 6169–6171.

CLOUTIER, P. A., SANDEL, B. R., ANDERSON, H. R., PAZICH, P. M. and SPIGER, R. J. (1973): Measurement of auroral Birkeland currents and energetic particle fluxes. J. Geophys. Res., **78**, 640–647.

D'ANGELO, N. (1973): Type III spectra of the radar aurora. J. Geophys. Res., **78**, 3987–3990.

DE LA BEAUJARDIERE, O., VONDRAK, R. and BARON, M. (1977): Radar observations of electric fields and currents associated with auroral arcs. J. Geophys. Res., **82**, 5051–5062.

FARLEY, D. T., JR. (1963): A plasma instability resulting in field-aligned irregularities in the ionosphere. J. Geophys. Res., **68**, 6083–6097.

FEJER, B. G. and KELLEY, M. C. (1980): Ionospheric irregularities. Rev. Geophys. Space Phys., **18**, 401–454.

HENDEL, H.W. and YAMADA, M. (1974): Identification of ion-cyclotron drift instability with discrete and continuous spectra. Phys. Rev. Lett., **33**, 1076–1079.

KELLEY, M. C. and MOZER, F. S. (1973): Electric field and plasma density oscillations due to the high-frequency Hall current two-stream instability in the auroral *E* region. J. Geophys. Res., **78**, 2214–2221.

KINDEL, J. M. and KENNEL, C. F. (1971): Topside current instabilities. J. Geophys. Res., **76**, 3055–3078.

MCDONALD, B. E., COFFEY, T. P., OSSAKOW, S. and SUDAN, R. N. (1974): Preliminary report of numerical simulation of type 2 irregularities in the equatorial electrojet. J. Geophys. Res., **79**, 2551–2554.

MIYAZAKI, S., OGAWA, T. and MORI, H. (1981): Observational results of electron density profile by S-310JA-7 rocket. Mem. Natl Inst. Polar Res., Spec. Issue, **18**, 300–303.

MOORCROFT, D. R. (1979): Dependence of radio aurora at 398 MHz on electron density and electric field. Can. J. Phys., **57**, 687–697.

OGAWA, T., MORI, H. and MIYAZAKI, S. (1975): Electron density irregularities observed in the Antarctic auroral *E* region. J. Radio Res. Labs., **22**, 1–21.

OGAWA, T., MORI, H. and MIYAZAKI, S. (1976): Rocket observations of electron density irregularities in the Antarctic auroral *E* region. J. Geophys. Res., **81**, 4013–4015.

OGAWA, T., MORI, H. and MIYAZAKI, S. (1978): Electron density and temperature profiles in the Antarctic auroral ionosphere observed by sounding rockets. J. Radio Res. Labs., **25**, 73–94.

OGAWA, T., MAKINO, M., HAYASHIDA, S., YAMAGISHI, H., FUJII, R., FUKUNISHI, H., HIRASAWA, T. and NISHINO, M. (1981): Measurements of auroral electric fields with an Antarctic sounding rocket S-310JA-7. 1. DC electric field. Mem. Natl Inst. Polar Res., Spec. Issue, **18**, 355–378.

SATO, T. (1971): Non-linear theory of the cross-field instability, explosive mode coupling. Phys. Fluids, **14**, 2426–2435.

SATO, T. and OGAWA, T. (1976): Self-consistent studies of two-dimensional large-scale (~100 m) electrojet irregularities. J. Geophys. Res., **81**, 3248–3256.

SUDAN, R. N., AKINRIMISI, J. and FARLEY, D. T. (1973): Generation of small-scale irregularities in the equatorial electrojet. J. Geophys. Res., **78**, 240–248.

SUDAN, R. N. and KESKINEN, M. J. (1979): Theory of strongly turbulent two-dimensional convection of low-pressure plasma. Phys. Fluids, **22**, 2305–2314.

YAMAGISHI, H., FUKUNISHI, H., HIRASAWA, T. and OGAWA, T. (1981): Measurements of auroral electric fields with an Antarctic sounding rocket S-310JA-7. 2. AC electric field. Mem. Natl Inst. Polar Res., Spec. Issue, **18**, 379–390.

(Received August 25, 1980; Revised manuscript received October 27, 1980)